

Effect of strain on structure and electronic properties of monolayer C_4N_4

Hao Chen, Ying Xu, Jia-Shi Zhao, and Dan Zhou

Citation: Chin. Phys. B, 2024, 33 (**5**): 057302. DOI: 10.1088/1674-1056/ad260c
Journal homepage: http://cpb.iphy.ac.cn; http://iopscience.iop.org/cpb

What follows is a list of articles you may be interested in

Anomalous valley Hall effect in two-dimensional valleytronic materials

Hongxin Chen(陈洪欣), Xiaobo Yuan(原晓波), and Junfeng Ren(任俊峰)
Chin. Phys. B, 2024, 33 (**4**): 047304. DOI: 10.1088/1674-1056/ad1c59

Improving the electrical performances of InSe transistors by interface engineering

Tianjun Cao(曹天俊), Song Hao(郝松), Chenchen Wu(吴晨晨), Chen Pan(潘晨), Yudi Dai(戴玉頓), Bin Cheng(程斌), Shi-Jun Liang(梁世军), and Feng Miao(缪峰)
Chin. Phys. B, 2024, 33 (**4**): 047302. DOI: 10.1088/1674-1056/ad24d7

Recent progress on valley polarization and valley-polarized topological states in two-dimensional materials

Fei Wang(王斐), Yaling Zhang(张亚玲), Wenjia Yang(杨文佳), Huisheng Zhang(张会生), and Xiaohong Xu(许小红)
Chin. Phys. B, 2024, 33 (**1**): 017306. DOI: 10.1088/1674-1056/ad0713

Magnetic and magnetotransport properties of layered $TaCoTe_2$ single crystals

Ming Mei(梅明), Zheng Chen(陈正), Yong Nie(聂勇), Yuanyuan Wang(王园园), Xiangde Zhu(朱相德), Wei Ning(宁伟), and Mingliang Tian(田明亮)
Chin. Phys. B, 2023, 32 (**12**): 127303. DOI: 10.1088/1674-1056/acd10a

Perspectives of spin-valley locking devices

Lingling Tao(陶玲玲)
Chin. Phys. B, 2023, 32 (**10**): 107306. DOI: 10.1088/1674-1056/acc809

Effect of strain on structure and electronic properties of monolayer C_4N_4

Hao Chen(陈昊)[1], Ying Xu(徐瑛)[1], Jia-Shi Zhao(赵家石)[2,†], and Dan Zhou(周丹)[1,‡]

[1] *School of Physics, Changchun University of Science and Technology, Changchun* 130022, *China*
[2] *School of Computer Science and Technology, Changchun University of Science and Technology, Changchun* 130022, *China*

(Received 17 November 2023; revised manuscript received 26 January 2024; accepted manuscript online 5 February 2024)

The first-principles calculations are performed to examine structural, mechanical, and electronic properties at large strain for a monolayer C_4N_4, which has been predicted as an anchoring promising material to attenuate shuttle effect in Li–S batteries stemming from its large absorption energy and low diffusion energy barrier. Our results show that the ideal strengths of C_4N_4 under tension and pure shear deformation conditions reach 13.9 GPa and 12.5 GPa when the strains are 0.07 and 0.28, respectively. The folded five-membered rings and diverse bonding modes between carbon and nitrogen atoms enhance the ability to resist plastic deformation of C_4N_4. The orderly bond-rearranging behaviors under the weak tensile loading path along the [100] direction cause the impressive semiconductor–metal transition and inverse semiconductor–metal transition. The present results enrich the knowledge of the structure and electronic properties of C_4N_4 under deformations and shed light on exploring other two-dimensional materials under diverse loading conditions.

Keywords: two-dimensional materials, strain effect, structural evolution, electronic properties

PACS: 73.90.+f ,77.80.bn, 83.10.Tv, 87.15.Pc **DOI:** 10.1088/1674-1056/ad260c

1. Introduction

Two-dimensional (2D) materials including graphene, silicene, metal oxides, transition-metal dichalcogenides, and transition-metal carbides, have received much attention in the fields of physics, chemistry, and materials science, especially in battery materials, because of their outstanding physical and chemical properties, such as high surface–volume ratio and unique electronic band structure, charge carrier mobility, and mechanical properties.[1–7] Lithium–sulfur (Li–S) battery has potential wide-ranging applications as the next-generation energy storage devices but the shuttle effect adversely influences battery longevity and performance.[8] Graphene, as the best known 2D carbon-based material, is hindered by the relatively low adsorption energy to be a high-performance anchoring material restraining the shuttle effect.[9,10] Recently, extensive research has shown that N-doped carbon materials with larger adsorption energy can attract lithium polysulfides (LiPSs) and thus improve the cycling performance of the batteries,[11,12] in which the newly predicted C_4N_4 monolayer phase with C_1 symmetry exhibits the larger absorption energy and lower diffusion energy barrier as an excellent anchoring material for Li–S batteries.[13] The C_4N_4 phase possesses a folded structure with two atomic layers and is mainly composed of C_3N_2 five membered rings. In addition, each row of five membered rings is connected with two nitrogen atoms.[13]

As an anchoring material, the stability of structural, mechanical, and electronic properties must be considered in practical application. C_4N_4 monolayer phase requires systematic and in-depth study to elucidate the atomistic mechanisms that determine key mechanical properties and to explore the other related properties under the complex application conditions. When exerting an external force on a material, the structure will try to resist the external force by the cohesive forces to avoid deformation, which is defined as stress. Tensile and shear stress refer to different types of structural responses that occur when two exerted forces pull in opposite directions, *i.e.*, the two forces are parallel to each other but in opposite directions. The relationship between stress and strain (stress–strain curves) provides the most fundamental information in strain engineering. Strain engineering is widely used to modulate the above properties in a controllable manner, which has developed into an efficacious strategy to enhance functional performance for electronic devices[14–18] and the stress–strain relation has developed the important means to depict mechanical properties of materials. Shear strains under appropriate compression constraints cause a surprising structural softening, triggering off an uncharacteristic ductile smooth flow in the rigid diamond crystal.[19–21] The applied external strain makes the electronic band structures near the Fermi level for dense H_3S vary significantly, correspondingly changing the superconducting critical temperature.[22] It is crucial to understand the electronic band structure of monolayer C_4N_4 under ambient pressure and additional uniaxial tension or pure shear strain along different directions.

To understand the stress responses and underlying atomistic deformation mechanisms along different loading conditions, we carry out comprehensive and systematical first-principles calculations of quasi-static stress–strain relations. According to the obtained results, we find that the ideal

†Corresponding author. E-mail: zhaojiashi@cust.edu.cn
‡Corresponding author. E-mail: zhoudan@cust.edu.cn

© 2024 Chinese Physical Society and IOP Publishing Ltd

strengths for C_4N_4 under tensile and pure shear deformation conditions can reach 13.9 GPa and 12.5 GPa, respectively. We calculate band gap at equilibrium and some key points of strain along the weaker directions to examine the effect of external strain on the electronic band gap. Our results demonstrate that external stress does play a considerable effect on the band gap, which is mainly reflected from the non-monotonic change in the [100] tensile strain as well as the reducing variation in the (100) [010] pure shear strain. In addition, the underlying mechanism of the change in band gap is analyzed based on the evolution of the electronic band structure near the Fermi level under external strain. Our findings reveal excellent mechanical and electronic properties of the C_4N_4 phase, indicating that it may have great potential in further nanoscale device manufacturing and application.

2. Computational methods

The first-principles calculations of stress–strain relation and electronic property were performed by using density functional theory (DFT)[23] as implemented in the Device Studio program, providing a number of functions for performing visualization, modeling and simulation. And DSPAW software was used and integrated into the Device Studio program.[24–26] The generalized gradient approximation (GGA) proposed by the Perdew–Burke–Ernzerhof (PBE) was adopted for the exchange–correlation functional.[27] The projector augmented wave (PAW) method was used to describe the electron–ion interaction,[28] where the $2s^22p^2$ and $2s^22p^3$ electrons are taken as the valence electrons for C and N atoms, respectively. To ensure an energy convergence and residual forces within 1 meV per atom and 1 meV·Å^{-1}, all of the calculated properties used plane-wave cutoff energy of 550 eV and the special points sampling integration over the Brillouin zone (BZ) was employed by using the Monkhorst–Pack (MP) method with $7 \times 4 \times 1$ special *k*-point meshes for structural optimization and $11 \times 8 \times 1$ special *k*-point meshes for band calculation.[29] The phonon dispersion along the high-symmetry points in the Brillouin zone was computed by using a 5×3 supercell. *Ab initio* molecular dynamics (AIMD) simulation to evaluate its thermal stability in a relatively large 5×3 supercell (120 atoms) was performed for 12 ps in steps of 1.0 fs at 300 K–2400 K in the simulation. The stress–strain relation was obtained through calculating the stress response to structural deformation along a series of specific loading directions combined with the quasi-static relaxation method.[30–33] The quasi-static relaxation method was used to simulate all kinds of loading conditions and determine the corresponding ideal strength and deformation mode.

3. Results and discussion

To verify the dynamic stability and thermal stability of C_4N_4, we have carry out the phonon dispersion and AIMD simulations at different temperatures. The results show that there is no imaginary frequency phonon mode as shown in Fig. 1(a), which indicates that C_4N_4 is dynamically stable. The mean square displacement (MSD) results show that the monolayer C_4N_4 remains stable below 2100 K during the simulation in Fig. 1(b). To examine the fundamental structural and electronic properties, we have systematically calculated stresses, local bonding patterns and bandgap variations associated with strains. We first examine the tensile deformation behavior by first-principles calculations of the tensile stress–strain relationship along the typical [100] and [010] high-symmetry direction, as illustrated in Fig. 2(a). The calculated peak stresses are 13.9 GPa and 14.8 GPa at strain $\varepsilon = 0.07$ and 0.17, respectively, indicating that the [100] tensile direction is weaker. At a small strain (below the strain of 0.07), the two stress–strain curves almost show an approximately linear relationship. When the elastic deformation reaches the limit, there will be a turning point in the tensile curve, which means that the atoms slip from the original lattice position to the new position to obtain the minimum total energy of the system. The stress–strain curve along the weaker [100] direction exhibits a non-monotonic trend with the further increase of strain (first decreases from 13.9 GPa to 4.9 GPa and then increases to 9.2 GPa). In addition, under the tensile condition of [100], when the strains reach 0.08 and 0.20 respectively, there is significant stress release in C_4N_4 phase.

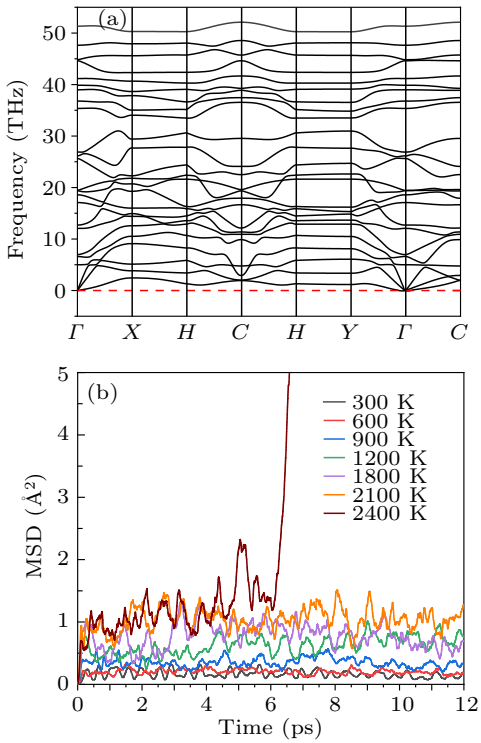


Fig. 1. (a) Phonon dispersion of C_4N_4, (b) time-dependent mean-squared displacements (MSD) for atomic positions of carbon in C_4N_4 at 300 K–2400 K.

For better clarifying the underlying mechanism, we now analyze the related atomic deformation mode under the [100]

tensile strain. Figures 2(b)–2(e) clearly show the transformation of the chemical bond transition before and after the stress critical point in the direction of the easy tensile deformation. When the strain increases from the value of 0.00 to 0.08, the layer thickness decreases from the value of 0.378 Å to 0.000 Å together with the fracture of the N–N bond. However, the further rising tensile strain leads to the enhancement of the layer thickness. For example, the layer thickness is 0.164 Å at a strain of 0.15. When the strain continues to increase to 0.20, the C–C bond breaks and the layer thickness rises to 0.838 Å, exceeding the equilibrium value. The ups and downs of the stress range after the peak value considerably enhances the ability of crystal to resist ductile deformation,[34,35] increasing the toughness of C_4N_4.

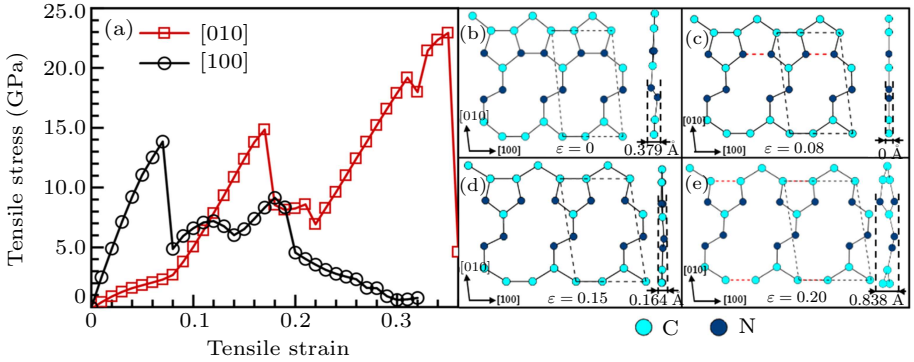


Fig. 2. (a) Stress–strain curves of C_4N_4 in the [010] tensile direction and [100] tensile direction, and (b)–(e) structural snapshots of C_4N_4 deformed in [100] tensile direction at key strain points.

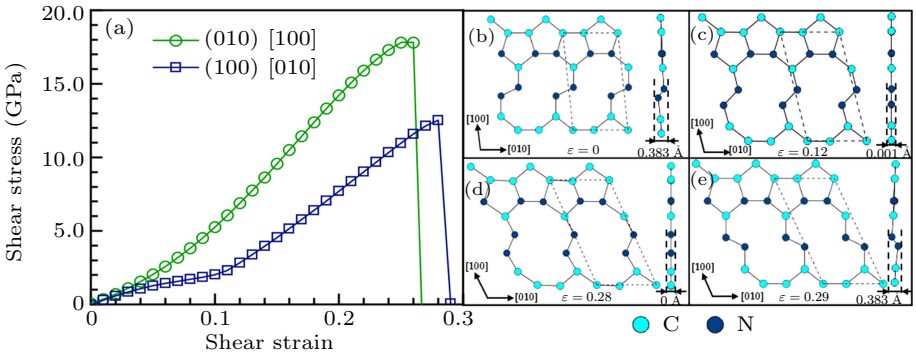


Fig. 3. (a) Stress–strain curves of C_4N_4 in (010) [100] direction and (100) [010] pure shear direction, and (b)–(e) structural snapshots of C_4N_4 deformed in (100) [010] pure shear direction at key strain points.

Then, we explore stress–strain relations of C_4N_4 under pure shear loading conditions along the (010) [100] and (100) [010] crystal directions. When subjected to pure shear strain, the two stress–strain curves both rise rapidly, reaching their high peak stresses. When exceeding the peak stress, a precipitous drop appears, which can be seen normally in strong covalent crystals in the shear direction,[36,37] leading to the failure of the original crystal structure. Figure 3(a) shows that the weaker shear stress response occurs along the deformation path in the (100) plane with [010] direction, with the peak stress of 12.5 GPa at a strain of 0.28, which is almost the same as the peak value of 13.9 GPa in the [100] tensile direction. This phenomenon is similar to that of diamond and *c*-BN, and they also have ideal tensile and shear strengths close to each other.[36,37] For another pure shear direction, the shear peak value is 17.8 GPa in the (010) [100] shear direction, which is 42% greater than the value obtained in the (100) [010] direction. Figure 3(a) indicates that C_4N_4 exhibits large anisotropy in its peak shear stress under pure shear mode. Despite the large anisotropy in the peak stress, the stress–strain relation shows that an isotropic behavior at small strain with visible deviation starts to occur at about 3% shear strain.[38] Interestingly, the current results show that strong structural deformation of the monolayer C_4N_4 occurs under strain loading, stemming from the corresponding modulation of its chemical bond length and bond angle. According to these results, we present in Figs. 3(b)–3(e) the structural snapshots of the strained C_4N_4 crystal structures, showcasing the detailed bond-weakening process and bond-breaking process of C_4N_4 along the weaker (100) [010] direction. It is noteworthy that the C_4N_4 structure retains its original atomic arrangement and the deformation mode under pure shear strain is mainly manifested in the variation of layer thickness. As the strain rises, the layer thickness first decreases from 0.383 Å to 0.000 Å and then increases to 0.383 Å.

To assess the effect of external strain on electronic properties, we calculate the band gap of C_4N_4 under tensile strain as presented in Fig. 4(a). The anomalous structural deformation of monolayer C_4N_4 has profound influence on its electronic properties. In the present monolayer C_4N_4, various

strains are continuously loaded, coincidentally lead the electronic bandgap to decrease under the small loading conditions. The increase of the strain along the [010] tensile direction suppresses the band gap and then reopens the band gap as the tensile strain further increases. The C_4N_4 phase remains non-metallic throughout the [010] tensile strain. It is obvious that more significant structural changes occur along the [100] tensile direction than under the other loading conditions. As the [100] tensile strain increases, the stress decreases quickly after having passed through the peak value of 13.9 at strain $\varepsilon = 0.07$ driven by the breaking mechanism of partial N–N bonds, which is shown in Fig. 2(c). Recent theoretical calculations indicate that the application of strain can cause the bond length to significantly elongate, thereby breaking symmetry, splitting and broadening band, and even metalize insulators and semiconductors, *e.g.*, diamond and solid molecular hydrogen. Our results show that the band gap initially decreases along the [100] direction with tensile strain rising, and the metallization of C_4N_4 is achieved at strain $\varepsilon = 0.08$, driven by the mechanism of bandgap closure along several high-symmetry directions, which coincides with a sudden increase of elongation of the N–N bonds at the same tensile strain. As the [100] tensile strain increases from 0.08 to 0.20, the C–C bonds become the main load resistance, generating a second elastic response regime. A significant structural deformation accompanied by the sudden breaking of part of C–C bonds and gradual increasing the layer thickness results in bandgap reopening at the tensile strain from 0.20 to 0.22.

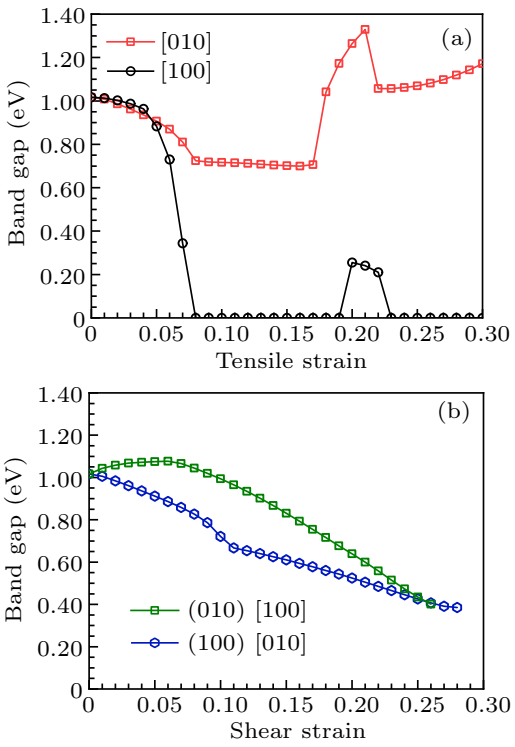


Fig. 4. Electronic band gap of deformed C_4N_4 along (a) tensile and (b) pure shear paths.

This bandgap closing-reopening process occurs along with the switching of band-state characteristic between the conduction band minimum (CBM) and valence band maximum (VBM) as shown in the orbit-resolved band structure shown in Fig. 5. At equilibrium, the C_4N_4 phase is a semiconductor with a band gap of 1.02 eV, as presented in Fig. 5(a), which is slightly larger than the previously calculated value of 0.618 eV,[13] because a larger kinetic energy cutoff is used in the current calculation. It is worthy to mention that the standard density functional calculations tend to underestimate the band gap of semiconductor by about 30%, thus its true band gap can reach 1.5 eV, leading to the potential optical applications in water splitting and sunlight absorption.

When the tensile strain rises from 0.08 to 0.19, the overlap between the conduction band and the valence band makes C_4N_4 structure metallic, confirming the occurrence of metallization. Particularly, there is an energy band crossing the Fermi level in the range between the *X*–*H*–*C* direction and the *C*–*H*–*Y* direction, which gives rise to hole pockets and flat bands as indicated in Figs. 5(b) and 5(c). This overlap shrinks with strain increasing and vanishes at a strain of 20%. The tensile strain drives C_4N_4 into a semiconductor with an indirect band gap of 0.25 eV at a strain of 0.20 as shown in Fig. 5(d). These results suggest that the deformed C_4N_4 can be tuned by external strain to go through a sequence of semiconductor, metal, semiconductor, and metal transition under the [100] tensile strain.

We have also performed calculations to examine the electronic band gap variation under pure shear crystal directions including (010) [100] and (100) [010]. The results are presented in Fig. 4(b), revealing that the band gap of C_4N_4 is sensitive to the change of external pure shear strain. As the pure shear strain increases, the band gap of C_4N_4 decreases in magnitude along two different shear directions. For C_4N_4 phase under pure shear strain, there is no appearance of a semiconductor-to-metal transition through the closure of a band gap. The evolution of the band structure of C_4N_4 provides a better description of the band gap variation. When subjected to shear strain, due to the symmetry breaking, the VBM and the CBM around the BZ boundary along the Γ–*X* direction repel each other. The band structures, especially those near the Fermi energy, decrease due to the reduction of the bandwidth by shear strain. When the strain rises to 0.12, the deformed C_4N_4 is converted into a semiconductor with an indirect band gap of 0.65 eV as shown in Fig. 6(a). As the shear strain further increases, the deformed structure is still a narrow-band gap semiconductor with an indirect band gap of 0.39 eV as indicated in Fig. 6(b).

The present findings offer the important structure information of C_4N_4 under the tensile and shear loading for investigating adsorption, diffusion, and transport of LiPSs of the strained C_4N_4, and relative research analyses and methods may extend to a broad range of other 2D materials.[39,40] Strain offers a new effective tool to engineer materials for electrochemical properties, *e.g.*, less than 0.1% strain on an Ni-based metal–oxide nanostructure leads to anodic and cathodic

peak potential shifts of about 30 mV in an electrochemical cell.[41] Our results show that the anomalous structural deformation of the monolayer C_4N_4 has profound influence on its electronic properties, which is expected to improve its electrochemical performance by strain engineering, instead of searching or synthesizing new phases in this material family. However, the studies of the strain-modulated electro-chemistry in the monolayer C_4N_4 are beyond the scope of the present work. Recently, the experimental studies[41–44] showed that the material failure of nanomaterials with significantly reduced internal defects and surface flaws mainly depends on the intrinsic limits of atomic bonds, so the strain and strength obtained experimentally are close to the theoretical limits, such as the ultrahigh elastic strain of diamond nanoneedles (13.4%), and 15% strain of an Ni–Ti–O-based metaloxides formed on the superelastic shape memory NiTi alloys. Thus, the maximum elastic strain and strength of this type of C_4N_4 nanosheet system is expected to be achievable by further skilled experimental measurements.

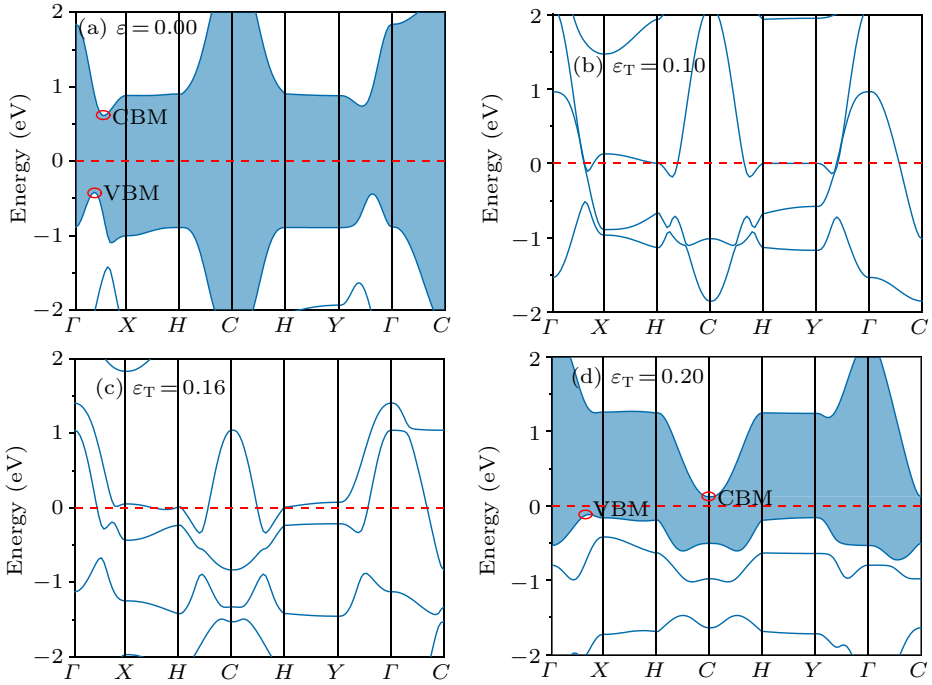


Fig. 5. Calculated electronic band structures of C_4N_4 at (a) equilibrium, (b) 10%, (c) 16%, and (d) 20% tensile (T) strain along [100] direction, respectively.

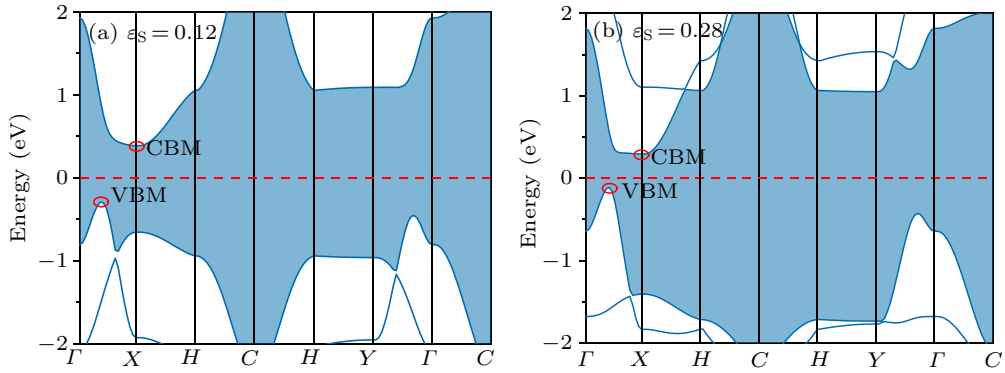


Fig. 6. Calculated electronic band structures of C_4N_4 under (a) 12% and (b) 28% shear (S) strain along the (100) [010] direction, respectively.

4. Conclusions

In this work, we have employed the first-principles calculationsto obtain the stress relationship under tensile and shear loading conditions and the directly related strain-induced electronic band structures for C_4N_4, a potential high-performance anchoring material for Li–S batteries. The folded five-membered rings and diverse bonding modes between carbon atom and nitrogen atom facilitate orderly bond-rearranging after stress peak value, which enhances the ability to resist plastic deformation, thereby increasing the toughness of C_4N_4 under tensile loading paths. C_4N_4 possesses a structure with two atomic layers, so C_4N_4 can retain the original atomic arrangement under pure shear strain, only manifesting in the variation of layer thickness. The tensile strain causes the impressive semiconductor–metal and inverse semiconductor–metal transition of deformed C_4N_4. The calculated electronic band

structures indicate that the C_4N_4 is still an indirect band gap semiconductor under shear strain. The present results provide the essential structure information of C_4N_4 under tensile and shear loading for further probing adsorption, diffusion, and transport of LiPSs of strained C_4N_4 and relative research analysis are suitable for extending to a broad range of other 2D materials.

Acknowledgements

We thank HZWTECH for providing computation facilities, and also thank Xiaowen Shi from HZWTECH for his useful help and discussion.

Project support by the National Natural Science Foundation of China (Grant Nos. 11704044 and 12074140).

References

[1] Xu R, Zhai H, Wang D, Song X Q, Zhou D and Li Q 2023 *ACS Mater. Lett.* **5** 2747
[2] Gu Z, Yu S, Xu Z, Wang Q, Duan T, Wang X, Liu S, Wang H and Du H 2022 *Chin. Phys. B* **31** 086107
[3] Li Y, Zhu S, Wu E, Ding H, Lu J, Mu X, Chen L, Zhang Y, Palisaitis J, Chen K, Li M, Yan P, Persson P O Å, Hultman L, Eklund P, Du S, Kuang Y, Chai Z and Huang Q 2023 *J. Phys. Chem. Lett.* **14** 481
[4] Shen J, Duan Q, Miao J, He S, He K, Dai W and Lu C 2023 *Chin. Phys. B* **32** 096302
[5] Fan Y, Li L, Zhang Y, Zhang X, Geng D and Hu W 2022 *Adv. Funct. Mater.* **32** 2111357
[6] Geim A K and Novoselov K S 2007 *Nat. Mater.* **6** 183
[7] Hu C W, Yang Y, Hou C and Liang T X 2021 *Comput. Mater. Sci.* **194** 110424
[8] Yuan H, Zhang W, Wang J G, Zhou G, Zhuang Z, Luo J, Huang H, Gan Y, Liang C, Xia Y, Zhang J and Tao X 2018 *Energy Storage Mater.* **10** 1
[9] Li X and Zhi L 2018 *Chem. Soc. Rev.* **47** 3189
[10] Shao B, Jiang X, Berges J, Meng S and Huang B 2023 *Chin. Phys. Lett.* **40** 087303
[11] Luo Y, Wu M, Zhang D, Liu J, He Y, Zhang W, Liu S, Dong Y, Xiang C, Yang L, Liu H, Shu H, Wang X and Chen M 2023 *ACS Sustain. Chem.* **11** 1087
[12] He C, Liang Y and Zhang W 2022 *ACS Appl. Mater. Interfaces* **14** 29120
[13] Li T, He C and Zhang W 2019 *J. Mater. Chem. A* **7** 4134
[14] Sun C, Guo W and Yao Y 2022 *Chin. Phys. Lett.* **39** 087101
[15] Miao Y, Zhao Y, Zhang S, Shi R and Zhang T 2022 *Adv. Mater.* **34** 2200868
[16] Liu C, Song X, Li Q, Ma Y and Chen C 2021 *Chin. Phys. Lett.* **38** 086301
[17] Liu C F and Wang J 2022 *Chin. Phys. Lett.* **39** 077301
[18] Ma J J, Wang Z Y, Xu S G, Gao Y X, Zhang Y Y, Dai Q, Lin X, Du S X, Ren J D and Gao H J 2022 *Chin. Phys. Lett.* **39** 047403
[19] Liu L, Zhang S and Zhang H 2022 *Chin. Phys. Lett.* **39** 056102
[20] Liu C, Song X, Li Q, Ma Y and Chen C 2019 *Phys. Rev. Lett.* **123** 195504
[21] Liu C, Song X, Li Q, Ma Y and Chen C 2020 *Phys. Rev. Lett.* **124** 147001
[22] Liu C, Zhai H, Sun Y, Gong W, Yan Y, Li Q and Zheng W 2018 *Phys. Chem. Chem. Phys.* **20** 5952
[23] Kohn W and Sham L J 1965 *Phys. Rev.* **140** A1133
[24] Hongzhiwei Technology D S, Version 2021A, China, 2021. Available online: https://iresearch.net.cn/cloudSoftware
[25] Wang Z, Li Z, Zhang Y and Liu W 2020 *J. Chem. Phys.* **153** 164109
[26] Blöchl P E 1994 *Phys. Rev. B* **50** 17953
[27] Perdew J P, Burke K and Ernzerhof M 1996 *Phys. Rev. Lett.* **77** 3865
[28] Kresse G and Joubert D 1999 *Phys. Rev. B* **59** 1758
[29] Monkhorst H J and Pack J D 1976 *Phys. Rev. B* **13** 5188
[30] Pan Z, Sun H and Chen C 2007 *Phys. Rev. Lett.* **98** 135505
[31] Pan Z, Sun H, Zhang Y and Chen C 2009 *Phys. Rev. Lett.* **102** 055503
[32] Ogata S, Li J, Hirosaki N, Shibutani Y and Yip S 2004 *Phys. Rev. B* **70** 104104
[33] Roundy D, Krenn C R, Cohen M L and Morris J W 1999 *Phys .Rev. Lett.* **82** 2713
[34] An Q, Goddard W A and Cheng T 2014 *Phys. Rev. Lett.* **113** 095501
[35] Han Z, Liu H, Li Q, Zhou D and Lv J 2021 *Chin. Phys. Lett.* **38** 046201
[36] Zhang Y, Sun H and Chen C 2006 *Phys. Rev. B* **73** 144115
[37] Telling R H, Pickard C J, Payne M C and Field J E 2000 *Phys. Rev. Lett.* **84** 5160
[38] Liang H, Li H, Li Q and Chen C 2020 *Phys. Rev. B* **102** 134105
[39] Fang R, Lu C, Chen A, Wang K, Huang H, Gan Y, Liang C, Zhang J, Tao X, Xia Y and Zhang W 2020 *ChemSusChem* **13** 1409
[40] Carvalho A, Wang M, Zhu X, Rodin A S, Su H and Neto A C 2016 *Nat. Rev. Mater.* **1** 16061
[41] Muralidharan N, Carter R, Oakes L, Cohn A P and Pint C L 2016 *Sci. Rep.* **6** 27542
[42] Amit B, Daniel B, Zhang H T, Muk-Fung Y, Liu J B, Dong J C, Ding F, Lu J, Dao M, Zhang W J, Lu Y and Subra S 2018 *Science* **360** 300
[43] Anmin N, Bu Y Q, Li P H, Zhang Y Z, Jin T Y, Liu J B, Zhang S, Wang Y B, He J L, Liu Z Y, Wang H T, Tian Y J and Yang W 2019 *Nat. Commun.* **10** 5533
[44] Dang C, Chou J P, Dai B, Chou C T, Yang Y, Fan R, Lin W, Meng F, Hu A, Zhu J. Han J, Minor A M, Li J and Lu Y 2021 *Science* **371** 76